# Separation of an aqueous mixture of 6-kestose/sucrose with zeolites: A molecular dynamics simulation

Iria Bolaño Losada [a], Pablo Grobas-Illobre [a], Alechania Misturini [a], Julio Polaina [b], Yohanna Seminovski [a], German Sastre [a],*

[a] *Instituto de Tecnología Química, Universitat Politécnica de Valéncia, Avda. de los Naranjos s/n, 46022, Valencia, Spain*
[b] *Instituto de Agroquímica y Tecnología de Alimentos, CSIC, Av. Agustín Escardino 7, Paterna, 46980, Valencia, Spain*

## ARTICLE INFO

## ABSTRACT

Extra-large pore zeolites are a small subset (21) among the whole list of 253 zeolites available. The discovery of new low-glycemic sugars is very attractive as new healthy additives in the food field. This is the case of the 6-kestose. In the present case, it appears in a mixture in aqueous solution together with sucrose, the separation of the mixture being necessary. For this, we have focused on using certain zeolites with adequate pore sizes that allow the separation of this mixture, considering that since the molecular size of 6-kestose is greater than sucrose, it is necessary to promote the sorption of the latter, so that the first can be purified. After a computational screening of micropores of the 253 IZA zeolites, 11 zeolites were selected. Of these, 3 extra-large pore zeolites (AET, DON, ETR) have been proposed, which were analyzed in-depth through a molecular dynamics study considering the external surface. The results show that DON presents the most promising theoretical results for a selective sucrose/6-kestose separation.

## 1. Introduction

Zeolites constitute a substantial family of crystalline materials, whose application covers different fields, such as catalysis, separations, ion exchangers, and adsorbents [1]. Their structure is shaped by a three-dimensional tetrahedral periodic framework, from which a high porosity arises due to the nanometer-sized channels that they host. This feature, combined with their wide surface area, explains their adsorption properties. Thus, they are used as molecular sieves for the separation of molecules and ions, being the microporous size of the structures that defines their size-separation capacity [2,3]. At the present time, 253 different zeolite framework types have been described, and can be found at the International Zeolite Association (IZA) website [4].

The presence of hydrophilic silanol surface groups and aluminum atoms locally compensate for the rest of the silica framework which is hydrophobic. The presence of hydrophilic centres creates the possibility to selectively adsorb polar molecules. In particular, water molecules interact with the oxygens of the zeolite framework through H-bonding and also with Brønsted sites in the zeolite, if present, through the water oxygens. Additional effects may be achieved regarding selectivity, which can be due not to the chemical nature of the framework but rather

due to the topology of the micropores in what is usually called 'shape selectivity'. This phenomena favours the adsorption of molecules, through van der Waals interactions, when their shape is similar to that of the micropore [5].

Computer simulations approaches based in a combination of classical force fields and molecular dynamics (MD), are considered an outstanding tool to tackle the theoretical evaluations concerning diffusion [6–9]. The use of MD allows to study the evolution of a molecule of interest with time, under specific selected conditions while analyzing a wide area of the potential energy surface involved, conditions which might be chosen so its direct comparison or application to an experimental problem [10]. Regarding the use of a flexible zeolite framework, it has been cautioned in several publications that the calculation of the diffusion coefficients from these studies are really sensitive to the force field used [11,12].

Using separation technology, zeolites can be suggested as key materials in glucose-fructose separation. The adsorption of carbohydrates in the liquid phase has been successfully investigated in hydrophobic Y zeolites where the pores of the zeolite are enriched with the saccharide molecules and there is therefore a high specific adsorption of carbohydrates [13]. Beta zeolites have also been shown to have similar effects

---

[14,15]. The use of zeolites in the chromatographic separation of carbohydrates has been investigated for the separation of the mixture glucose-fructose [16–18], glucose-sucrose-sorbitol [19] and oligosaccharides of fructose [20]. In addition, the adaptation of FAU zeolite to replace organic polymeric resins as inorganic ion exchangers was investigated in the separation of isomaltose-oligosaccharide saccharide mixture in a liquid chromatography [21].

6-Kestose is an oligosaccharide of industrial interest because of its prebiotic and other functional properties. Consequently, efficient procedures for the production of this sugar have been devised [22]. A significant technical problem of the production procedure is the need to purify 6-kestose from sucrose. The separation of sucrose and 6-kestose in zeolites modelized in this study is just a representative example whose results could be applied to the separation of other oligosaccharides obtained by enzymatic synthesis, a procedure which is gaining industrial relevance [23]. In the present work, the capability of different zeolites for the separation of a sucrose/6-kestose mixture in aqueous solution has been evaluated.

In the separation of 6-kestose and sucrose, as well as other oligosaccharides, sugar concentration and temperature are crucial parameters. For practical reasons (productivity), sugar concentration, limited by solubility (an intrinsic property of each sugar, which is a function of temperature), should be as high as possible. An optimum temperature should be selected that maximizes sugar solubility, stability and energy saving. Approaching boiling point temperature risks sugar denaturalization either by Maillard reaction or caramelization [24]. The presence of amino acids, causing Maillard reaction, in oligosaccharide preparations obtained by enzymatic synthesis should be taken into account. Zeolites can be an alternative to nanofiltration, currently used industrially for oligosaccharide separation [25].

Taking advantage of the large variety of pore sizes in zeolites, we explore whether there are suitable candidates for the separation of sugars. We employ the IZA (International Zeolite Association) database and a definition of *ad hoc* parameters that may maximize the separation in order to select candidates [4]. After a short list was generated, MD simulations of sugars in a selection of candidate zeolites allowed us to estimate if there are large differences in the mobility of the sugars selected.

## 2. Methodology and models

### 2.1. Sucrose and 6-kestose geometries for diffusion

Sucrose and 6-kestose are two relatively large molecules whose conformations, in molecular dynamics simulations, are expected to give rise to a variability in their corresponding molecular size, which in turn will influence whether or not the sugar molecules can fit in different zeolite micropores. As a first estimation, their molecular size was roughly estimated, using a recently developed algorithm, from the ground state geometries obtained through first-principles calculations using the Gaussian16 package [26].

Density functional theory (DFT) geometry optimizations were performed with the B3LYP [27] exchange-correlation hybrid functional and the Pople-type 6-311G basis set [28]. Grimme's D3 empirical dispersion correction [29,30] were also included to account for van der Waals interactions. Geometry optimizations were performed without including the effect of solvent (water).

Once ground state geometries (Fig. 1) have been obtained, molecular size has been calculated with the 'shoebox' algorithm [31]. The algorithm finds the two atoms of maximum intramolecular distance and makes a rotation to define a new x axis along those two atoms, and calculates maximum intramolecular distances along two axes (y,z) perpendicular to x. In the new coordinate system, the maximum and minimum coordinates over the three axes define a box (xmax−xmin, ymax−ymin, zmax−zmin) of nearly minimum size (similarly to shoe boxes), and whose values, ordered from largest to shortest are our
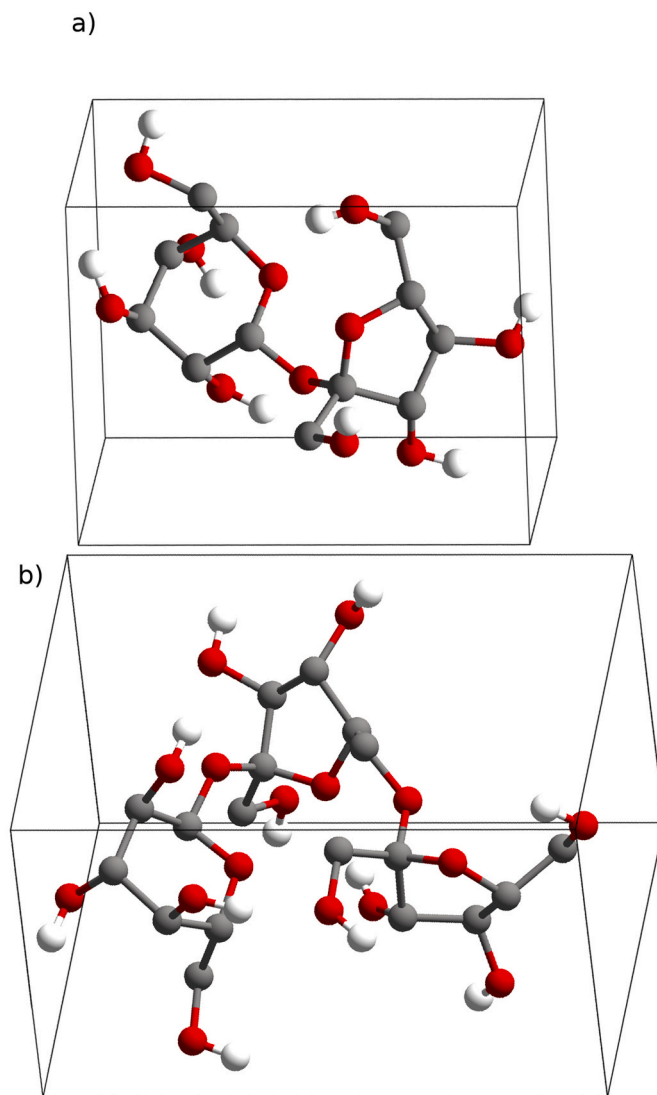
a)



b)

**Fig. 1.** Structures of the sugar molecules framed by shoebox algorithm. a) sucrose ($C_{12}H_{22}O_{11}$) disaccharide showing cyclohexane (glucose) and cyclopentane (fructose) rings; and b) 6-kestose ($C_{18}H_{32}O_{16}$) trisaccharide, showing cyclohexane (glucose) and 2 cyclopentane (fructose) rings. The dimensions $\Phi$(x, y,z), in Å, are $\Phi_S$: (9.4, 7.5, 6.3) for sucrose and $\Phi_K$: (11.4, 9.1, 6.7) for 6-kestose. Atoms colors are O: red, C: gray, H: white. For the sake of clear visualization, aliphatic hydrogens were omitted. (For interpretation of the references to color in this figure legend, the reader is referred to the Web version of this article.)

definition of molecular size ($\Phi$). The results obtained (in Å) are $\Phi_S$: 9.4, 7.5, 6.3 for sucrose and $\Phi_K$: 11.4, 9.1, 6.7 for 6-kestose molecules.

A configuration search study [32] was carried out to find how molecular size (and hence fitting in zeolite pores) can be affected by sugar conformations. Details are given in Section S1 of Supporting Information. The molecular size of selected configuration (Fig. 1) is representative of the configurations found during the search and can be considered a valid estimation to assess candidate zeolites for separation of the sugars.

### 2.2. Selection of potential zeolites for sucrose/6-kestose separation

The main objective of this work is to find an appropriate zeolite to separate 6-kestose and sucrose. Target zeolites should allow the diffusion of sucrose and preclude 6-kestose. A first selection of zeolites has been made by comparing micropore size with sugar dimensions.

Micropore size has been tabulated according to the maximum diameter of a sphere that can diffuse (along a,b,c crystallographic directions), defined according to Foster et al. [33], available from the IZA Atlas [4]. Molecular size has been calculated according to the 'shoebox' algorithm, as explained in the above section (Fig. 1). Molecular diffusion proceeds with the molecule aligned with the diffusion channel, hence only 'y' and 'z' dimensions need to be compared with the micropore size. For diffusion to be allowed, y and z should be smaller than one (or more) zeolite channel dimension (either a, b, or c). For diffusion to be precluded, y or z should be larger than all zeolite micropore dimensions (a, b and c). Applying these criteria to all 253 zeolites in the IZA database, a selection of 11 (Table 1) was made that, in principle, may allow the diffusion of sucrose and preclude the diffusion of 6-kestose. The zeolites are: AET, DON, EMT, ETR, FAU, IFO, MOZ, SBE, SBS, SBT, and UTL (Fig. 2).

### 2.3. Molecular dynamic simulation

Molecular dynamics was performed using the DL_POLY program (version 2.20) [34]. The force field of Bushuev and Sastre [5] was employed for zeolite frameworks, consisting of a harmonic expression for three body interactions, along with Coulomb and Lennard-Jones potentials for the nonbonded interactions. When the zeolite surface was modeled, H–O bonds of silanol groups were defined by a Morse potential [10]. A flexible version of the SPC model [35] was employed for the water molecules, proposed for zeolite systems in aqueous media [5]. Sucrose and 6-kestose bonded terms described bond stretching and bending with harmonic expressions, and torsional barriers by a truncated Fourier series, as defined by Oie et al. forcefield [36]. The point charges assigned to sugar atoms were computed by the Gasteiger-Marsili method [37] as implemented in Open Babel [38]. van der Waals interactions between sugar atoms came from the UFF force field [39], while its interaction with zeolite were considered as reported by Kiselev and co-workers [40,41]. The remaining Lennard-Jones parameters needed were obtained by applying Lorentz-Berthelot combination rules. A complete force field description can be found in the Supporting Information (Section S2).

Systems were simulated in the NVT ensemble, where the constant temperature of 338 K was ensured by Evans thermostat [42]. Periodic boundary conditions were applied to avoid finite box-size effects. For the nonbonded forces, a cutoff of 9.0 Å was considered, and the Ewald summation was applied to deal with long-range interactions. Considering a time step of 1.0 fs, simulation boxes were equilibrated for 20 ps, thereafter the trajectories were calculated for either 10 (bulk) or 20 (membrane) ns, with time evolution being computed by the Velocity Verlet algorithm. Diffusion coefficients were calculated (Supporting Information, section S3) for the bulk systems using the data from the first 5 ns of the mean square displacement plots.

Two types of systems (Table 2) were simulated, called bulk and membrane, corresponding to increasing accuracy. 'Bulk' models contain the usual 3-D zeolite periodic model without external surface and one sugar molecule is located inside the micropore, with all atoms of the system (between 729 and 2277) allowed to relax and their trajectories being recorded for 10 ns. 'Membrane' models contain two zeolite layers separated by 20 Å, producing two reservoirs, with sugar molecules initially located in one of these reservoirs, outside the zeolite, and were run for 20 ns Some zeolite atoms were fixed in order to keep the zeolite layer separation since, otherwise, both tend to approximate each other. Zeolite layers were terminated by silanol groups which were allowed to relax. To obtain more realistic results, water molecules were added to all systems, using packmol software [43], to simulate the aqueous solution in which the sugar separation process should be performed. The water content could not be calculated according to the expected uptake since no water isotherms on these systems are available. Instead, a water content was selected so that full solvation of sugar molecules was achieved and the water density was 0.98 g/cm$^3$. Selected membrane systems were simulated during 20 ns for simulation boxes with low (four sucrose and four 6-kestose) and high sugar loading (nine sucrose and nine 6-kestose for ETR; twelve sucrose and twelve 6-kestose for AET and DON).

## 3. Results

### 3.1. Mobility of sucrose and 6-kestose in AET, DON, EMT, ETR, FAU, IFO, MOZ, SBE, SBS, SBT, UTL zeolites

As a first insight into the mobility of sugars in the 11 candidate zeolites (AET, DON, EMT, ETR, FAU, IFO, MOZ, SBE, SBS, SBT, UTL), 10 ns molecular dynamics in bulk systems with only one sugar molecule were performed (Table 2). Although 10 ns is a moderately large simulation time, having only one sugar molecule in the unit cell will preclude obtaining valuable statistics, and these calculations will be taken only to qualitatively guess the most promising zeolites for sucrose/6-kestose separation.

Figs. 3 and 4 show the mobility of sucrose and 6-kestose in the different zeolites. Mobility itself will not be used as main criterium, but rather diffusion coefficients, obtained from mobility-related parameters (mean square displacements versus time), will be used. Although displacements are small, only a qualitatively different mobility for sucrose, larger than that for 6-kestose is needed in order to select the corresponding system for a more in-depth study that will assess more accurately the possible separation of sucrose/6-kestose mixtures. Figs. 3 and 4 show a similar mobility for sucrose and 6-kestose except in the cases of DON, AET, ETR and IFO.

In AET and ETR a clearly larger mobility for sucrose than 6-kestose can be observed. In DON, although the mobility of sucrose is small,
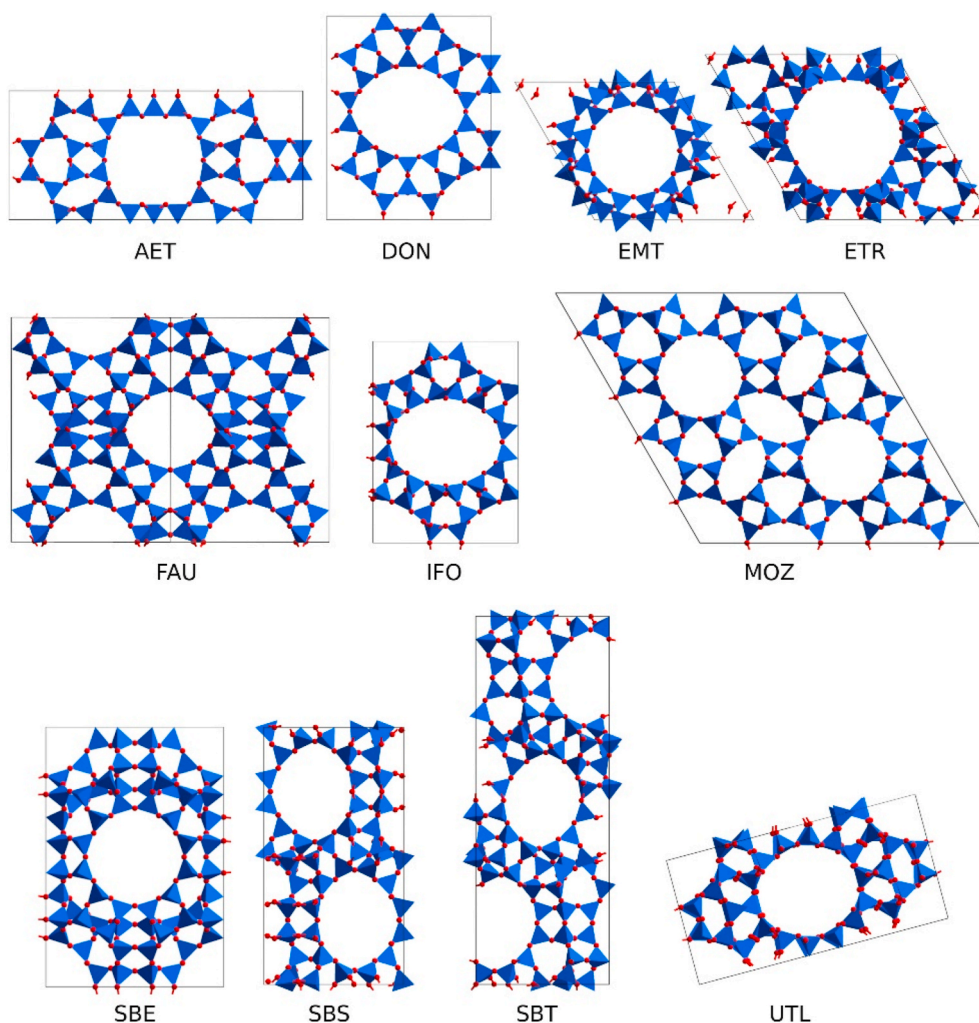
**Table 1**

Preliminary analysis of 11 zeolites for sucrose and 6-kestose separation. Micropore data for zeolites includes: maximum diameter of sphere that can be included (d), maximum diameter of sphere that can diffuse in directions a, b, c (relevant values in bold), channel size (Å), and ring size. Sucrose diffusion will be allowed if $\Phi_S(y,z)$ (Fig. 1) is equal or smaller than zeolite diffusion channel. 6-kestose diffusion will be precluded if $\Phi_K$(y and/or z) (Fig. 1) is larger than zeolite diffusion channel.

| Zeolite | Micropore Size (Å) | | | | | | Molecular size (Å, Fig. 1) and comparison with micropore size | |
|---|---|---|---|---|---|---|---|---|
| | d | a | b | c | channel size | ring size | $\Phi_S$: 9.4, 7.5, 6.3 | $\Phi_K$: 11.4, 9.1, 6.7 |
| AET | 8.4 | 1.8 | 1.8 | **7.6** | 7.9×8.7 | 14 | $\Phi_S(y,z) \cong$ AET(c) | $\Phi_K(y) >$ AET(c) |
| DON | 8.8 | 2.2 | 1.8 | **8.1** | 8.1×8.2 | 14 | $\Phi_S(y,z) <$ DON(c) | $\Phi_K(y) >$ DON(c) |
| EMT | 11.6 | **6.5** | **6.5** | **7.4** | 7.3×7.3 | 12 | $\Phi_S(y,z) \cong$ EMT(a,b,c) | $\Phi_K(y) >$ EMT(a,b,c) |
| ETR | 10.1 | 2.9 | 2.9 | **9.3** | 10.1×10.1 | 18 | $\Phi_S(y,z) <$ ETR(c) | $\Phi_K(y,z) <$ ETR(c) |
| FAU | 11.2 | **7.4** | **7.4** | **7.4** | 7.4×7.4 | 12 | $\Phi_S(y,z) \cong$ FAU(a,b,c) | $\Phi_K(y) >$ FAU(a,b,c) |
| IFO | 7.8 | **7.2** | 2.0 | 1.1 | 9.3×10.6 | 16 | $\Phi_S(y,z) \cong$ IFO(a) | $\Phi_K(y) >$ IFO(a) |
| MOZ | 10.0 | 3.4 | 3.4 | **7.5** | 6.8×7.0 | 12 | $\Phi_S(y,z) \cong$ MOZ(c) | $\Phi_K(y) >$ MOZ(c) |
| SBE | 12.5 | **7.3** | **7.3** | 3.9 | 7.2×7.4 | 12 | $\Phi_S(y,z) \cong$ SBE(a,b) | $\Phi_K(y) >$ SBE(a,b) |
| SBS | 11.5 | **7.3** | **7.3** | 5.7 | 6.9×7.0 | 12 | $\Phi_S(y,z) \cong$ SBS(a,b) | $\Phi_K(y) >$ SBS(a,b) |
| SBT | 11.2 | **7.3** | **7.3** | 5.7 | 7.3×7.8 | 12 | $\Phi_S(y,z) \cong$ SBT(a,b) | $\Phi_K(y) >$ SBT(a,b) |
| UTL | 9.3 | 1.4 | 5.8 | **7.6** | 7.1×9.5 | 14 | $\Phi_S(y,z) \cong$ UTL(c) | $\Phi_K(y) >$ UTL(c) |

**Fig. 2.** Zeolite structures selected to study sucrose and 6-kestose diffusion. Views show the channel for diffusion in AET, DON, EMT, ETR, FAU, IFO, MOZ, SBE, SBS, SBT and UTL. Same scale is used for all figures.

**Table 2**
Models employed for the molecular dynamics simulations, specifying the number of silanol groups ($SiO_{3/2}H$) and silica units ($SiO_2$) of the zeolite, as well as the number of sucrose, 6-kestose, and water molecules. Bulk models (without silanols) contain only 1 sugar molecule, run for 10 ns, and were used for low accuracy calculations. Membrane models (those with silanols) run for 20 ns, and contain much larger unit cells, with number of sugar molecules being: 8 (AET, DON, ETR) at low loading (Section 3.2.1); and 18 (ETR) or 24 (AET, DON) at high loading (Section 3.2.2).

| Zeolite | $SiO_2$ | $SiO_{3/2}H$ | Suc | Kes | Water | Zeolite | $SiO_2$ | $SiO_{3/2}H$ | Suc | Kes | Water |
|---------|---------|--------------|-----|-----|-------|---------|---------|--------------|-----|-----|-------|
| AET | 575 | 0 | 1 | 0 | 54 | SBE | 256 | 0 | 1 | 0 | 57 |
| AET | 575 | 0 | 0 | 1 | 56 | SBE | 256 | 0 | 0 | 1 | 55 |
| DON | 256 | 0 | 1 | 0 | 31 | SBS | 384 | 0 | 1 | 0 | 94 |
| DON | 256 | 0 | 0 | 1 | 30 | SBS | 384 | 0 | 1 | 0 | 92 |
| EMT | 384 | 0 | 1 | 0 | 99 | SBT | 576 | 0 | 1 | 0 | 140 |
| EMT | 384 | 0 | 0 | 1 | 97 | SBT | 576 | 0 | 0 | 1 | 133 |
| ETR | 192 | 0 | 1 | 0 | 36 | UTL | 304 | 0 | 1 | 0 | 54 |
| ETR | 192 | 0 | 0 | 1 | 37 | UTL | 304 | 0 | 0 | 1 | 48 |
| FAU | 192 | 0 | 1 | 0 | 52 | AET | 1728 | 288 | 4 | 4 | 3347 |
| FAU | 192 | 0 | 0 | 1 | 51 | DON | 1536 | 256 | 4 | 4 | 3150 |
| IFO | 384 | 0 | 1 | 0 | 113 | ETR | 1344 | 192 | 4 | 4 | 2400 |
| IFO | 384 | 0 | 0 | 1 | 111 | AET | 1728 | 288 | 12 | 12 | 3054 |
| MOZ | 648 | 0 | 1 | 0 | 89 | DON | 1536 | 256 | 12 | 12 | 2868 |
| MOZ | 648 | 0 | 0 | 1 | 89 | ETR | 1344 | 192 | 9 | 9 | 2190 |

the mobility of 6-kestose is extremely small. IFO is a representative case of zeolites in which, surprisingly, the mobility of 6-kestose is larger than that of sucrose. The small mobility of sucrose might be due to a nearly perfect match of O⋯H bonding between zeolite oxygens and alcohol hydrogens. With the larger 6-kestose, the fit would be less pronounced, leading to a larger mobility. Other zeolites in which this 'anomalous' behaviour of lower mobility for the smaller sugar is observed are FAU, MOZ, SBE, SBS, UTL.

Diffusion coefficients show low diffusivity, but the values obtained allow to confirm the conclusions above regarding the relative mobility
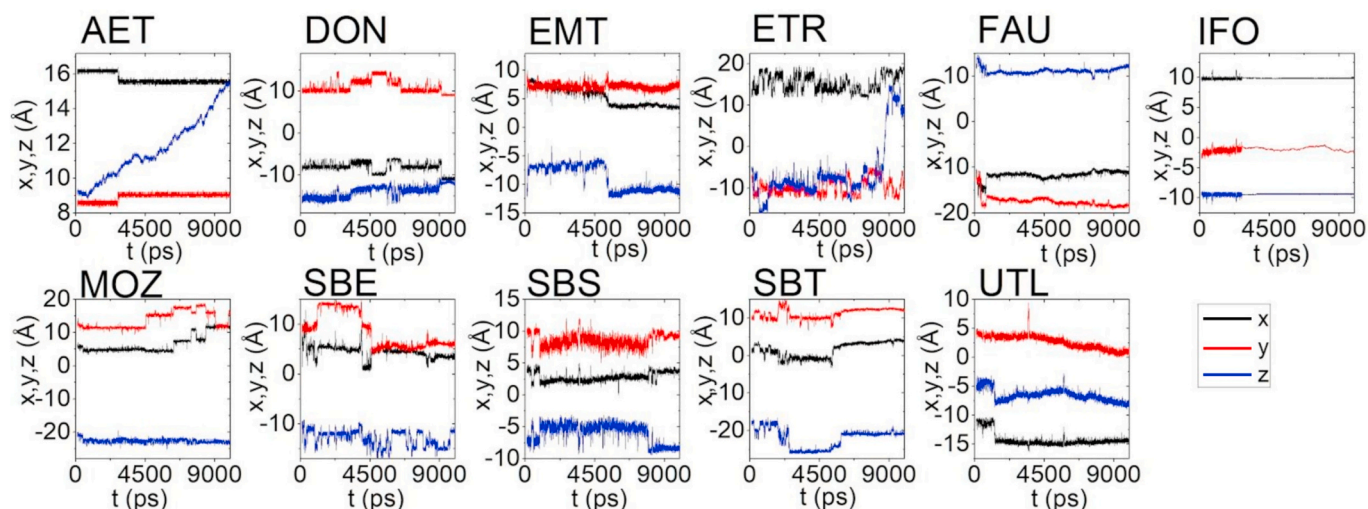
**Fig. 3.** Mobility of sucrose in: AET, DON, EMT, ETR, FAU, IFO, MOZ, SBE, SBS, SBT, UTL, at 338 K. All systems contain water molecules. Black, red and blue colors represent sucrose position in the x, y and z axis respectively. (For interpretation of the references to color in this figure legend, the reader is referred to the Web version of this article.)
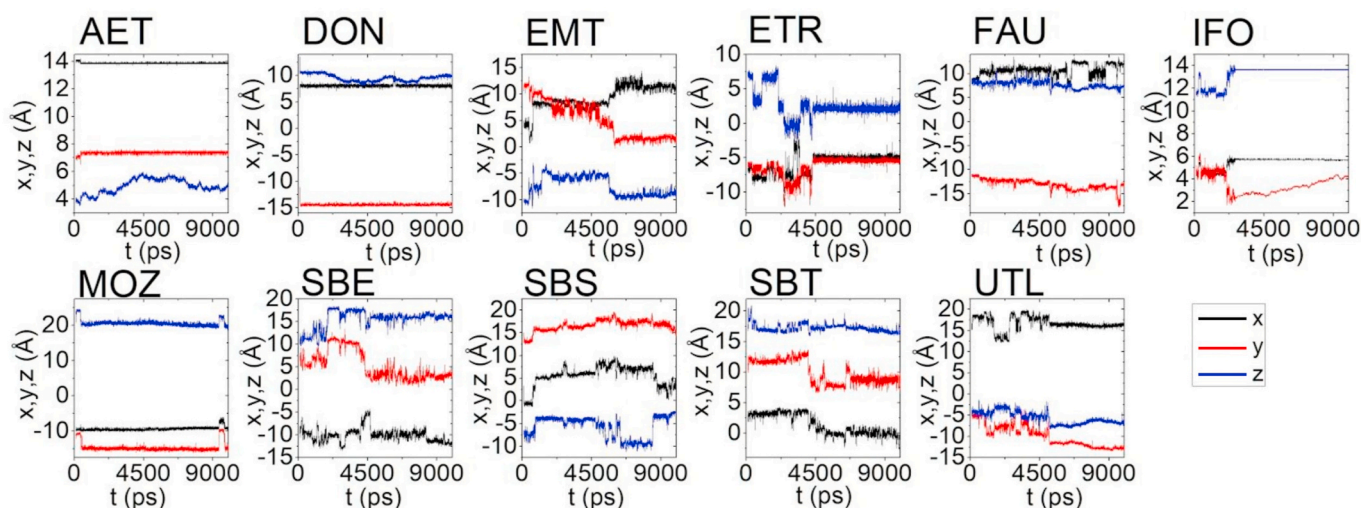


**Fig. 4.** Mobility of 6-kestose in: AET, DON, EMT, ETR, FAU, IFO, MOZ, SBE, SBS, SBT, UTL, at 338 K. All systems contain water molecules. Black, red and blue colors represent 6-kestose position in the x, y and z axis respectively. (For interpretation of the references to color in this figure legend, the reader is referred to the Web version of this article.)

of sugars. Mean square displacement plots are included in the Supporting Information (Section S3), from which diffusion coefficients have been obtained. For the purpose here, the ratio of diffusion coefficient sucrose/6-kestose in each zeolite is meaningful (Table 3). The values indicate a larger preliminary separation value for ETR, AET, DON, in agreement with the conclusion above. We have disregarded the subset of zeolites showing 'anomalous' behaviour (IFO, FAU, MOZ, SBE, SBS, UTL), with larger diffusivity for the bulkier sugar. In particular, IFO is not a good candidate since although having a large pore dimension, 9.3 × 10.6 Å, sufficient for diffusion of sucrose and 6-kestose, the largest sphere that can diffuse through IFO channels is much smaller (due to channel ellipticity), 7.2 Å along [100]. Hence, the zeolites selected for a more in-depth study of their capability for sucrose/6-kestose separation are: AET, DON, ETR.

The temperature selected for our molecular dynamics runs was 338 K, since it is the best temperature fulfilling the conditions of: i) being not too high, which would pose an economic penalty in any further possible application, and ii) being able to give sufficiently different mobility for sucrose and 6-kestose. Results at 298 K give too similar mobilities for

**Table 3**
Ratio of diffusion coefficients for sucrose/6-kestose in zeolites at 338 K.

| Zeolite | $D_S/D_K$ |
|---------|-----------|
| AET | 7.5 |
| DON | 4.8 |
| EMT | 0.9 |
| ETR | 8.5 |
| FAU | 0.8 |
| IFO | 0.01 |
| MOZ | 0.6 |
| SBE | 0.2 |
| SBS | 0.2 |
| SBT | 2.2 |
| UTL | 0.3 |

sucrose and 6-kestose, whilst temperatures of 378 K and higher do not give significant differences from the results shown here at 338 K. Results at 378 K are shown as Supporting Information.

Operating conditions at 338 K (chosen for this study) represent a convenient upper limit that maximizes sugar solubility and stability. Although degradation of sucrose and 6-kestose in an environment free of enzymes and acids is not expected to happen at the considered temperatures, it is safer to avoid large temperatures such as 378 K to avoid the risk of sugar denaturalization either by Maillard reaction or caramelization.

### 3.2. Uptake of sucrose/6-kestose mixture in AET, DON and ETR membranes

#### 3.2.1. Dilute sugar loading

The mobilities of sucrose and 6-kestose in the AET, DON and ETR membranes (Fig. 5) are shown in the Supporting Information (Section S4). Membranes have been created with the general strategy of allowing uptake of sucrose and 6-kestose in a realistic system in which a mixture of both sugars is present. In a first approach, 4 molecules of each sugar have been introduced near the external surface of the zeolite to improve statistics, instead of only one as in previous zeolite-bulk calculations. A sufficient number of water molecules has been introduced in each of the AET, DON and ETR systems (3347, 3150 and 2400, respectively, see Table 2), which have been distributed along all parts of the system (both reservoirs and channels of zeolite layers).

At low loading (4 sucrose and 4 6-kestose molecules) none of the membranes show significant uptake after 20 ns (Figs. 6 and 7). The reason is that sugar molecules interact strongly with the zeolite external surface and remain attached, with little probability to jump into the channel (Figs. S6–S9), in agreement with the so called 'surface barrier' effect [44].

Sugar adsorption over the zeolite surface is more energetically accessible rather than the sugar flow thought the zeolite cavity. At dilute solutions, the significant sugar-zeolite interaction in the surface hinders the sugar displacement through the zeolite. At increased loadings the external surface will become quickly saturated with a monolayer of sugar molecules, after which the incoming molecules will interact less strongly with the zeolite external surface and hence diffusion into the channel will become more probable. In our models this can be simulated

by increasing the sugar loading, which is compatible with its high solubility (2100 g/L for sucrose at 298 K [45]). Among the membranes investigated, ETR presents the thickest external surface (Fig. S10), that together with the number of silanol sites to anchor the sugar molecule, contributes to increase the barrier to enter the zeolite channel. More details of surface effects are analyzed in the Supporting Information (Section S5).

#### 3.2.2. Large sugar loading

In order to remove the effect of the surface barrier, two large loadings, 9 + 9 (ETR) and 12 + 12 (AET and DON) molecules of sucrose and 6-kestose were considered (Figs. 8 and 9).

An analysis was carried out of the sugar location throughout the 20 ns simulation, with detailed trajectories shown in Figs. S11–S13. A representative configuration is shown in Fig. 10 for each zeolite. It can be seen that sugar uptake is, in all three cases (AET, DON, ETR),
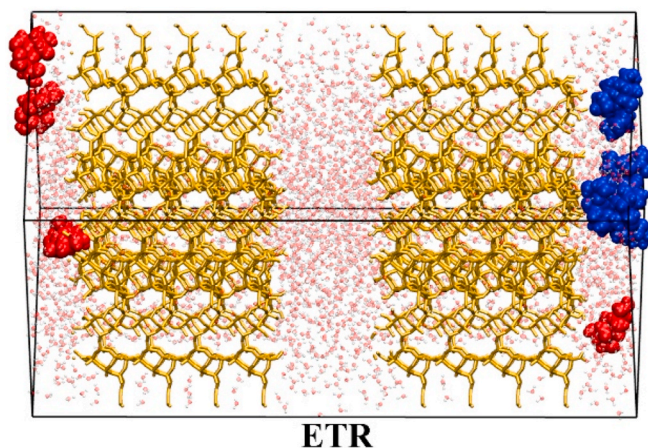


**Fig. 6.** Uptake of a low loading sucrose (red, 4 molecules)/6-kestose(blue, 4 molecules) mixture in water (transparent) in ETR membrane (yellow) at 338 K after 20 ns The figure shows no uptake at this low sugar loading after 20 ns
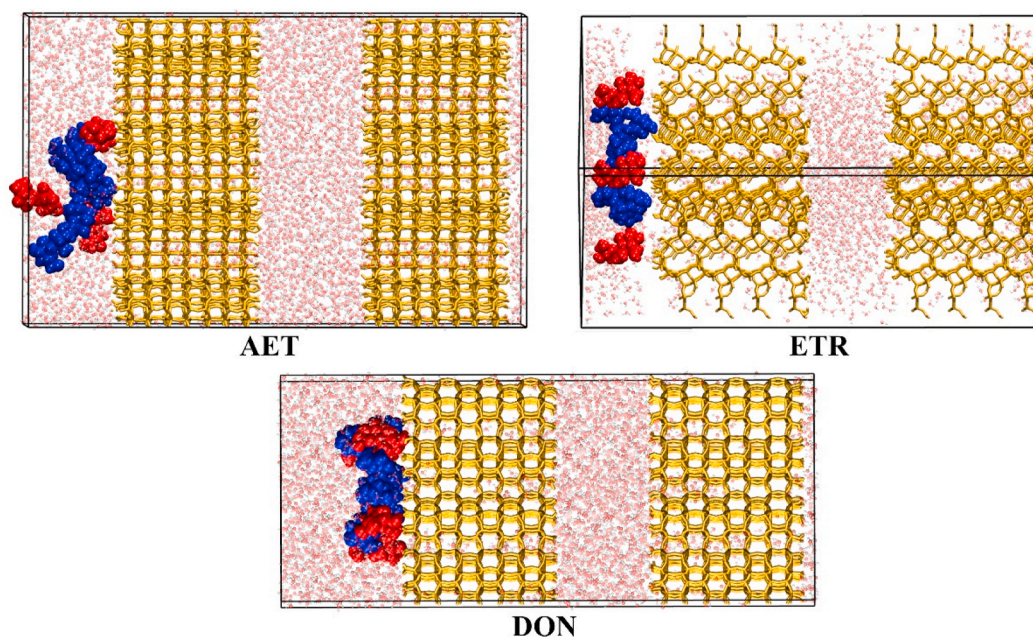


**Fig. 5.** Initial configurations of AET, DON and ETR membrane systems (yellow) containing two parallel layers (terminated by silanol groups) of ca. 31–36 Å thickness, separated by two reservoirs. Reservoir-1 (left) is initially filled with water (transparent), 4 sucrose (red) and 4 6-kestose (blue) molecules, whilst reservoir-2 (middle) is initially filled only with water molecules. Water molecules do also locate inside zeolite micropores. (For interpretation of the references to color in this figure legend, the reader is referred to the Web version of this article.)
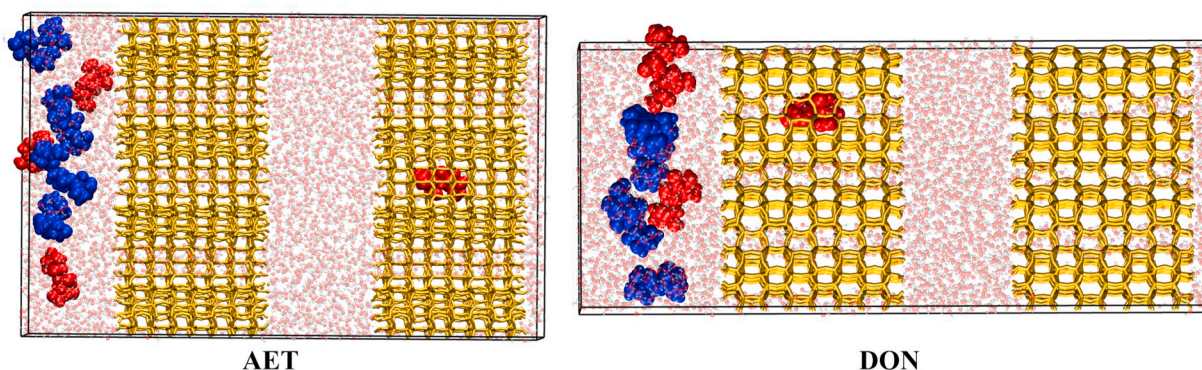
**Fig. 7.** Configuration showing the largest uptake of sucrose into AET (left) and DON (right) membranes (yellow) at 338 K after 20 ns with low sugar concentration (4 sucrose molecules in red, and 4 6-kestose molecules, in blue) in water (transparent). The figure shows a maximum uptake of 1 sucrose molecule at this low sugar loading. (For interpretation of the references to color in this figure legend, the reader is referred to the Web version of this article.)

preferentially observed for sucrose (red) whilst 6-kestose (blue) remains outside the zeolite, in reservoir-1. Although AET and ETR are selective for sucrose uptake, the flux of molecules does not seem particularly large. Nevertheless, DON shows not only a selective uptake of sucrose but also a very high molecular flux (Fig. 11), as can be seen from some molecules reaching, or being very close to, reservoir-2. The increase in sugar concentration substantially promoted the uptake and diffusion of sucrose into the three systems.

An attempt to rationalize the results in terms of pore size and surface effects is mandatory but not easy. These concepts are invoked, as in this study, in order to make a selection of candidates, but the quantitative results can only be found through the MD simulations. These three zeolites (AET, DON, ETR) already showed the largest diffusivity for sucrose with respect to 6-kestose (see Table 2). The pore size and largest sphere that can diffuse are largest for ETR (10.1 × 10.1 Å and 9.3 Å), hinting that ETR would show the largest flux, but this is not the case, perhaps due to an interaction zeolite-sugar less stabilizing when compared with a sucrose molecule tightly fitted in a channel. According to the relatively narrow values (7.9 × 8.7 Å and 7.6 Å), AET could be predicted as a zeolite with low flux and this is indeed found. For DON, the best system found, the pore size and largest sphere that can diffuse (8.1 × 8.2 Å and 8.1 Å) also indicate it should be a good candidate as it is indeed the case. Longer simulations and larger unit cells could give a

more accurate picture, but the current membrane models already give an excellent assessment and allow to confirm that the three zeolites (AET, DON, ETR) are good candidates for selective uptake of sucrose in a sucrose/6-kestose mixture. The MD calculations also indicate DON should be the best candidate due to the large and selective sucrose flux observed.

## 4. Discussion

Diffusion of sucrose and 6-kestose in extra-large pore zeolites is certainly slow, but still trends have been obtained and assessment of suitable structures for selective diffusion of sucrose has been possible. Both sugars considered, sucrose and 6-kestose, are large in size, with many degrees of freedom and a complex conformational space so that entering the zeolite channels becomes probabilistically difficult.

Bulk systems focus on the behaviour of sugar molecules once inside the micropores and were used as an intermediate step to focus on more realistic systems (that we called membranes) in which the role of the external surface is included. In fact, the role of the external surface (Supporting Information, Section S5) has been demonstrated to be crucial since large molecules do have a strong tendency to remain adsorbed on the external surface. This is one of the difficulties for entering the micropore, with the second difficulty being, as described
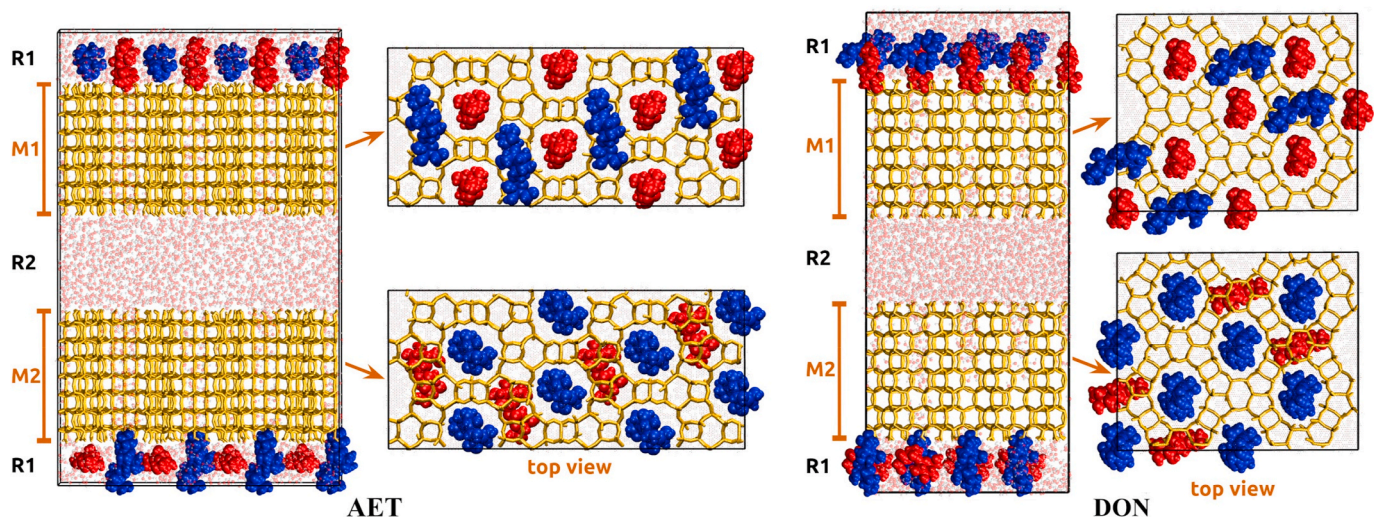


**Fig. 8.** Initial configuration of AET (left) and DON (right) membranes with the largest sugar loading, 12 sucrose (red) and 12 6-kestose (blue) molecules, in water (transparent). The MD simulations are carried out for 20 ns at 338 K. All sugar molecules are initially located at reservoir-1 (top and bottom part of the unit cell) whilst reservoir-2 (middle part of the unit cell) is initially empty of sugar molecules. (For interpretation of the references to color in this figure legend, the reader is referred to the Web version of this article.)
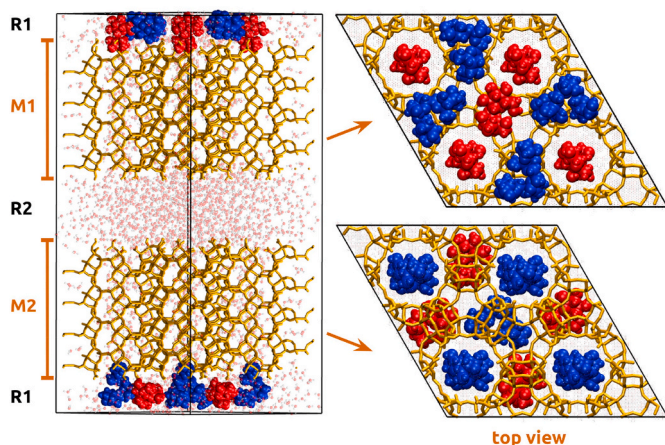
**Fig. 9.** Initial configuration of ETR membrane with large sugar loading, 9 sucrose (red) and 9 6-kestose (blue) molecules, in water (transparent). The MD simulations are carried out for 20 ns at 338 K. All sugar molecules are initially located at reservoir-1 (top and bottom part of the unit cell) whilst reservoir-2 (middle part of the unit cell) is initially empty of sugar molecules. (For interpretation of the references to color in this figure legend, the reader is referred to the Web version of this article.)

above, the conformational suitability needed between sugar and micropore. The third aspect is that adsorption at the external surface contributes to pore blocking. With 9.4 and 11.4 Å length for sucrose and 6-kestose, respectively, adsorption near the pore entrance (between 6.8 and 10.6 Å) can easily lead to pore blocking.

The sugar loading simulated in the membranes was deliberately chosen as not small. We tried in this way to include the effects of possible pore blocking and sugar-sugar interactions that appear at high sugar concentration. And indeed we were able to observe sugar (sucrose) uptake in the three best candidate membranes considered (AET, DON, ETR). The increase of loading was demonstrated to be a crucial effect. At larger than monolayer loading the sugar-surface interactions become weaker for those molecules outside the monolayer and this is the factor that allows sugar uptake. We have included a simple energetic analysis to illustrate this aspect (Supporting Information, Section S7).

Regarding the synthetic feasibility of the four materials selected, AET

[46] has been obtained as $AlPO_4$ composition and is hydrothermally stable at the temperature (338 K) suggested for the separation. DON is an even more convenient material since it can be synthesized as pure silica [47], with higher hydrothermal stability than AET. ETR [48] is so far not applicable to this separation since its chemical composition is a gallo-alumino-silicate with a considerably high content of Ga, Ga/(Si + Al + Ga) = 24%. Thin zeolite membranes, in particular with high-aspect-ratio nanosheets and uniform thickness, similar to those described with the simple models in this study, have been recently prepared in the group of Tsapatsis and have demonstrated excellent performance for the selective separation of p-xylene from a xylenes mixture [49].

Water molecules play a particularly important role through solvation of sugar molecules and interaction with external silanols, as described in previous work [50]. Sugar(surface)-water and sugar(micropore)-water radial distribution functions (Supporting Information, Section S6) show the different effects of sugar solvation. The uptake of sugars is heavily influenced by the presence of water. Water uptake (intrusion) in small and medium pore pure silica zeolites is very small at lower pressure than water saturation vapor pressure [51,52] and this is also what we find in the membrane systems studied. Although external silanols can be eliminated from the external surface [53] in order to make it more hydrophobic, presumably leading to a reduced surface barrier and larger uptake, it is so far less than obvious that this can be applied as a general procedure, and so we stick in our model to the typical silanol termination. The important role of water is confirmed by our simulations without water (not shown for the sake of brevity), which lead to lower sugar uptake. A similar result was found by Siong et al. [54] in the Monte Carlo simulation of uptake of an alcohol/water mixture in silicalite at 303 K.

## 5. Conclusions

Molecular dynamics simulations have been carried out to study the separation of a disaccharide (sucrose) from a trisaccharide (6-kestose) using zeolites. Taking into account the molecular size, $\Phi(x,y,z)$, of sucrose and 6-kestose, and using descriptors of micropore size, a preliminary list of 11 zeolites from the IZA Atlas has been selected. The selection is based on the principles that: i) from the 3 molecular lengths (across x,y,z), only the two smallest, $\Phi(y,z)$, are important since the
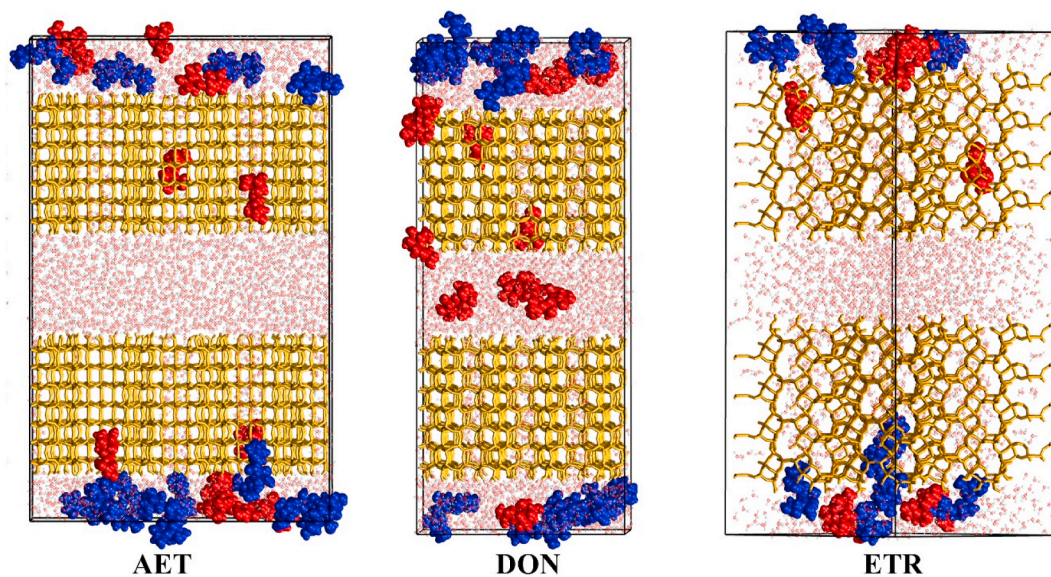


**Fig. 10.** Representative configurations showing sugar uptake into AET, DON and ETR membranes (yellow) with large loading of: 9 + 9 (ETR) and 12 + 12 (AET, DON) sucrose (red) and 6-kestose (blue) molecules. Water molecules shown with transparency. (For interpretation of the references to color in this figure legend, the reader is referred to the Web version of this article.)
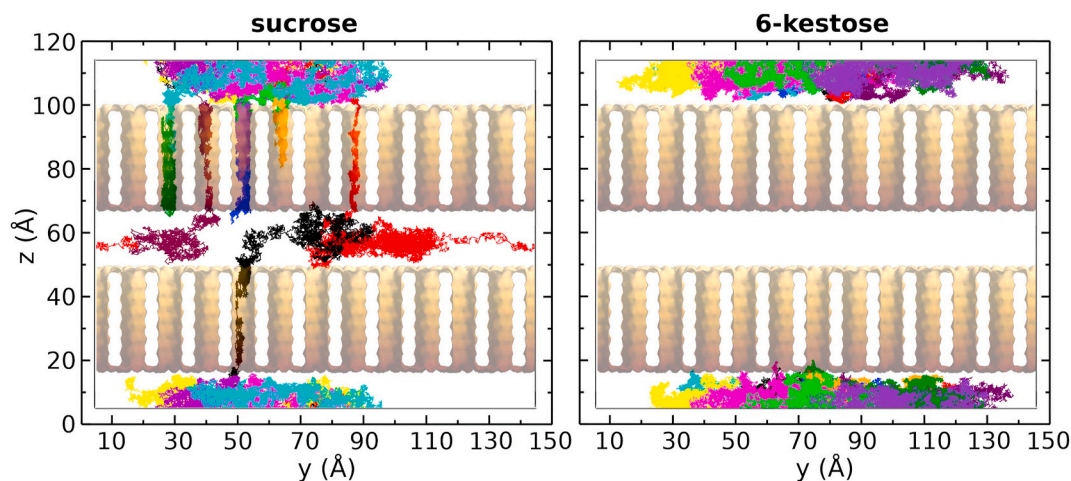
## sucrose                                6-kestose



**Fig. 11.** Sucrose (left) and 6-kestose (right) trajectories during MD simulation (at 338 K during 20 ns) of DON membrane in a mixture containing large sugar loading (12 sucrose and 12 6-kestose molecules).

longest goes parallel to the diffusing channel; ii) micropore size should be larger than Φ along y and z in order to allow diffusion; and iii) molecular size along diffusion (y or z) should be larger than micropore size for diffusion to be precluded.

Molecular dynamics simulations have been carried out for 10 ns in bulk models of the initial set of 11 zeolites, with each system containing only 1 molecule of either sucrose or 6-kestose, plus water molecules. These small systems give a qualitative estimation that allows to select 3 candidate zeolites in which a larger mobility is expected for sucrose than 6-kestose.

With the zeolite short list (AET, DON, ETR), more accurate molecular dynamics calculations have been performed in order to assess if a selective separation of sucrose/6-kestose might be possible. The larger accuracy did not consist in a long simulation time, but mainly in: i) including a 'membrane' zeolite model containing two reservoirs and two zeolite layers whose external surface is terminated by silanol groups; and ii) including a mixture of equal number of sucrose and 6-kestose molecules, and so the effect of the mixture is studied directly instead of the less accurate extrapolation from single component. Two different loadings were simulated for each case, chosen so that the large loading corresponds to a larger than monolayer adsorption. This facilitates the uptake by a decrease of the surface barrier effect leading to weaker sugar-surface interactions.

The calculations at large loading show that the three zeolites (AET, DON, ETR) are selective for sucrose uptake in the sucrose/6-kestose mixture. Finally, DON zeolite shows the largest flux, being therefore an excellent candidate for this separation process.

### Credit author contribution statement

IBL and PGI made molecular dynamics calculations and contributed to writing. YS contributed to editing the manuscript and molecular dynamics calculations of bulk systems. AM contributed to molecular dynamics calculations of membrane systems, editing the manuscript and writing the supporting information. JP contributed to the investigation outline. GS contributed to writing the manuscript, designed the membrane models, set up the computational methodology and supervised the molecular dynamics calculations.

### Declaration of competing interest

The authors declare that they have no known competing financial interests or personal relationships that could have appeared to influence the work reported in this paper.

### Acknowledgements

### Appendix A. Supplementary data

Supplementary data to this article can be found online at https://doi. org/10.1016/j.micromeso.2021.111031.

### References

[1] V. Van Speybroeck, K. Hemelsoet, L. Joos, M. Waroquier, R.G. Bell, C.R.A. Catlow, Advances in theory and their application within the field of zeolite chemistry, Chem. Soc. Rev. 44 (2015) 7044–7111, https://doi.org/10.1039/C5CS00029G.

[2] M. Wiśniewska, G. Fijałkowska, A. Nosal-Wiercińska, M. Franus, R. Panek, Adsorption mechanism of poly(vinyl alcohol) on the surfaces of synthetic zeolites: sodalite, Na-P1 and Na-A, Adsorption 25 (2019) 567–574, https://doi.org/10.1007/s10450-019-00044-2.

[3] N.V. Choudary, B.L. Newalkar, Use of zeolites in petroleum refining and petrochemical processes: recent advances, J. Porous Mater. 18 (2011) 685–692, https://doi.org/10.1007/s10934-010-9427-8.

[4] C. Baerlocher, L.B. McCusker, D.H. Olson, Atlas of Zeolite Frameworks Types, 6th revise, Elsevier, Amsterdam, 2007. http://www.iza-structure.org/databases. (Accessed 2 October 2020).

[5] Y.G. Bushuev, G. Sastre, Atomistic simulations of structural defects and water occluded in SSZ-74 zeolite, J. Phys. Chem. C 113 (2009) 10877–10886, https://doi.org/10.1021/jp9013306.

[6] A.F. Combariza, D.A. Gomez, G. Sastre, Simulating the properties of small pore silicazeolites using interatomic potentials, Chem. Soc. Rev. 42 (2013) 114–127, https://doi.org/10.1039/C2CS35243E.

[7] A.J. O'Malley, C.R.A. Catlow, Molecular dynamics simulations of longer n-alkanes in silicalite: a comparison of framework and hydrocarbon models, Phys. Chem. Chem. Phys. 15 (2013) 19024–19030, https://doi.org/10.1039/c3cp52653d.

[8] A.J. O'Malley, C.R.A. Catlow, Molecular dynamics simulations of longer n-alkanes in silicalite: state-of-the-art models achieving close agreement with experiment, Phys. Chem. Chem. Phys. 17 (2015) 1943–1948, https://doi.org/10.1039/C4CP04898A.

[9] B. Smit, T.L.M. Maesen, Molecular simulations of zeolites: adsorption, diffusion, and shape selectivity, Chem. Rev. 108 (2008) 4125–4184, https://doi.org/10.1021/cr8002642.

[10] A. Ghysels, S.L.C. Moors, K. Hemelsoet, K. De Wispelaere, M. Waroquier, G. Sastre, V. Van Speybroeck, Shape-selective diffusion of olefins in 8-ring solid acid microporous zeolites, J. Phys. Chem. C 119 (2015) 23721–23734, https://doi.org/10.1021/acs.jpcc.5b06010.

[11] A. García-Sánchez, D. Dubbeldam, S. Calero, Modeling adsorption and self-diffusion of methane in LTA zeolites: the influence of framework flexibility, J. Phys. Chem. C 114 (2010) 15068–15074, https://doi.org/10.1021/jp1059215.

[12] N.E.R. Zimmermann, S. Jakobtorweihen, E. Beerdsen, B. Smit, F.J. Keil, In-depth study of the influence of host−framework flexibility on the diffusion of small gas

molecules in one-dimensional zeolitic pore systems, J. Phys. Chem. C 111 (2007) 17370–17381, https://doi.org/10.1021/jp0746446.

[13] I. Fornefett, D. Rabet, C. Buttersack, K. Buchholz, Adsorption of sucrose on zeolites, Green Chem. 18 (2016) 3378–3388, https://doi.org/10.1039/C5GC02832A.

[14] C. Buttersack, I. Fornefett, J. Mahrholz, K. Buchholz, Specific adsorption from aqueous phase on apolar zeolites, Stud. Surf. Sci. Catal. 105 (1997) 1723–1730, https://doi.org/10.1016/S0167-2991(97)80636-2.

[15] S. Berensmeier, K. Buchholz, Separation of isomaltose from high sugar concentrated enzyme reaction mixture by dealuminated β-zeolite, Separ. Purif. Technol. 38 (2004) 129–138, https://doi.org/10.1016/j.seppur.2003.10.012.

[16] C.B. Ching, C. Ho, K. Hidajat, D.M. Ruthven, Experimental study of a simulated counter-current adsorption system-V. Comparison of resin and zeolite absorbents for fructose-glucose separation at high concentration, Chem. Eng. Sci. 42 (1987) 2547–2555, https://doi.org/10.1016/0009-2509(87)87006-9.

[17] C. Ho, C.B. Ching, D.M. Ruthven, A comparative study of zeolite and resin adsorbents for the separation of fructose-glucose mixtures, Ind. Eng. Chem. Res. 26 (1987) 1407–1412, https://doi.org/10.1021/ie00067a023.

[18] C.B. Ching, D.M. Ruthven, A liquid phase chromatographic study of sorption and diffusion of glucose and fructose in NaX and KX zeolite crystals, Zeolites 8 (1988) 68–73, https://doi.org/10.1016/S0144-2449(88)80032-0.

[19] P.K. Muralidharan, C.B. Ching, Determination of multicomponent adsorption equilibria by liquid chromatography, Ind. Eng. Chem. Res. 36 (1997) 407–413, https://doi.org/10.1021/ie9604278.

[20] R.C. Kuhn, F.M. Filho, Separation of fructooligosaccharides using zeolite fixed bed columns, J. Chromatogr. B 878 (2010) 2023–2028, https://doi.org/10.1016/j.jchromb.2010.05.039.

[21] W. Wach, I. Fornefett, C. Buttersack, K. Buchholz, Chromatographic separation of saccharide mixtures on zeolites, Food Bioprod. Process. 114 (2019) 286–297, https://doi.org/10.1016/j.fbp.2018.10.008.

[22] J. Marín-Navarro, D. Talens-Perales, J. Polaina, One-pot production of fructooligosaccharides by a Saccharomyces cerevisiae strain expressing an engineered invertase, Appl. Microbiol. Biotechnol. 99 (2015) 2549–2555, https://doi.org/10.1007/s00253-014-6312-4.

[23] D. Talens-Perales, J. Polaina, J. Marín-Navarro, Enzyme engineering for oligosaccharide biosynthesis, in: Front. Discov. Innov. Interdiscip. Microbiol., Springer India, 2015, pp. 9–31, https://doi.org/10.1007/978-81-322-2610-9_2.

[24] K.S. Woo, H.Y. Kim, I.G. Hwang, S.H. Lee, H.S. Jeong, Characteristics of the thermal degradation of glucose and maltose solutions, Prev. Nutr. Food Sci. 20 (2015) 102–109, https://doi.org/10.3746/pnf.2015.20.2.102.

[25] Z. Rizki, A.E.M. Janssen, A. van der Padt, R.M. Boom, Separation of fructose and glucose via nanofiltration in presence of fructooligosaccharides, Membranes 10 (2020) 298, https://doi.org/10.3390/membranes10100298.

[26] M.J. Frisch, G.W. Trucks, H.B. Schlegel, G.E. Scuseria, M.A. Robb, J.R. Cheeseman, G. Scalmani, V. Barone, G.A. Petersson, H. Nakatsuji, X. Li, M. Caricato, A. V. Marenich, J. Bloino, B.G. Janesko, R. Gomperts, B. Mennucci, H.P. Hratchian, J. V. Ortiz, A.F. Izmaylov, J.L. Sonnenberg, D. Williams-Young, F. Ding, F. Lipparini, F. Egidi, J. Goings, B. Peng, A. Petrone, T. Henderson, D. Ranasinghe, V. G. Zakrzewski, J. Gao, N. Rega, G. Zheng, W. Liang, M. Hada, M. Ehara, K. Toyota, R. Fukuda, J. Hasegawa, M. Ishida, T. Nakajima, Y. Honda, O. Kitao, H. Nakai, T. Vreven, K. Throssell, J.J.A. Montgomery, J.E. Peralta, F. Ogliaro, M.J. Bearpark, J.J. Heyd, E.N. Brothers, K.N. Kudin, V.N. Staroverov, T.A. Keith, R. Kobayashi, J. Normand, K. Raghavachari, A.P. Rendell, J.C. Burant, S.S. Iyengar, J. Tomasi, M. Cossi, J.M. Millam, M. Klene, C. Adamo, R. Cammi, J.W. Ochterski, R.L. Martin, K. Morokuma, O. Farkas, J.B. Foresmanand, D.J. Fox, Gaussian Inc., Wallingford CT, 2016.

[27] A.D. Becke, Density-functional thermochemistry. III. The role of exact exchange, J. Chem. Phys. 98 (1993) 5648–5652, https://doi.org/10.1063/1.464913.

[28] A.D. McLean, G.S. Chandler, Contracted Gaussian basis sets for molecular calculations. I. Second row atoms, Z =11–18, J. Chem. Phys. 72 (1980) 5639–5648, https://doi.org/10.1063/1.438980.

[29] S. Grimme, J. Antony, S. Ehrlich, H. Krieg, A consistent and accurate ab initio parametrization of density functional dispersion correction (DFT-D) for the 94 elements H-Pu, J. Chem. Phys. 132 (2010) 154104, https://doi.org/10.1063/1.3382344.

[30] S. Grimme, S. Ehrlich, L. Goerigk, Effect of the damping function in dispersion corrected density functional theory, J. Comput. Chem. 32 (2011) 1456–1465, https://doi.org/10.1002/jcc.21759.

[31] S. León, G. Sastre, Computational screening of structure-directing agents for the synthesis of pure silica ite zeolite, J. Phys. Chem. Lett. 11 (2020) 6164–6167, https://doi.org/10.1021/acs.jpclett.0c01734.

[32] N. Metropolis, A.W. Rosenbluth, M.N. Rosenbluth, A.H. Teller, E. Teller, Equation of state calculations by fast computing machines, J. Chem. Phys. 21 (1953) 1087, https://doi.org/10.1063/1.1699114.

[33] M.D. Foster, I. Rivin, M.M.J. Treacy, O. Delgado Friedrichs, A geometric solution to the largest-free-sphere problem in zeolite frameworks, Microporous Mesoporous Mater. 90 (2006) 32–38, https://doi.org/10.1016/j.micromeso.2005.08.025.

[34] W. Smith, T.R. Forester, DL_POLY_2.0: a general-purpose parallel molecular dynamics simulation package, J. Mol. Graph. 14 (1996) 136–141, https://doi.org/10.1016/S0263-7855(96)00043-4.

[35] H.J.C. Berendsen, J.P.M. Postma, W.F. van Gunsteren, J. Hermans, Interaction models for water in relation to protein hydration, in: B. Pullman (Ed.), Intermol. Forces, 1981, pp. 331–342, https://doi.org/10.1007/978-94-015-7658-1_21.

[36] T. Oie, G.M. Maggiora, R.E. Christoffersen, D.J. Duchamp, Development of a flexible intra- and intermolecular empirical potential function for large molecular systems, Int. J. Quant. Chem. 20 (1981) 1–47, https://doi.org/10.1002/qua.560200703.

[37] J. Gasteiger, M. Marsili, A new model for calculating atomic charges in molecules, Tetrahedron Lett. 19 (1978) 3181–3184, https://doi.org/10.1016/S0040-4039(01)94977-9.

[38] N.M. O'Boyle, M. Banck, C.A. James, C. Morley, T. Vandermeersch, G. R. Hutchison, Open Babel: an open chemical toolbox, J. Cheminf. 3 (2011) 33, https://doi.org/10.1186/1758-2946-3-33.

[39] A.K. Rappe, C.J. Casewit, K.S. Colwell, W.A. Goddard, W.M. Skiff, UFF, a full periodic table force field for molecular mechanics and molecular dynamics simulations, J. Am. Chem. Soc. 114 (1992) 10024–10035, https://doi.org/10.1021/ja00051a040.

[40] A.V. Kiselev, A.A. Lopatkin, A.A. Shulga, Molecular statistical calculation of gas adsorption by silicalite, Zeolites 5 (1985) 261–267, https://doi.org/10.1016/0144-2449(85)90098-3.

[41] C.R.A. Catlow, C.M. Freeman, B. Vessal, S.M. Tomlinson, M. Leslie, Molecular dynamics studies of hydrocarbon diffusion in zeolites, J. Chem. Soc., Faraday Trans. 87 (1991) 1947–1950, https://doi.org/10.1039/ft9918701947.

[42] L. Lue, O.G. Jepps, J. Delhommelle, D.J. Evans, Configurational thermostats for molecular systems, Mol. Phys. 100 (2002) 2387–2395, https://doi.org/10.1080/00268970210122145.

[43] L. Martínez, R. Andrade, E.G. Birgin, J.M. Martínez, PACKMOL: a package for building initial configurations for molecular dynamics simulations, J. Comput. Chem. 30 (2009) 2157–2164, https://doi.org/10.1002/jcc.21224.

[44] G. Sastre, J. Kärger, D.M. Ruthven, Molecular dynamics study of diffusion and surface permeation of benzene in silicalite, J. Phys. Chem. C 122 (2018) 7217–7225, https://doi.org/10.1021/acs.jpcc.8b00520.

[45] S.H. Yalkowsky, R.M. Dannenfelser, Aquasol Database of Aqueous Solubility, College of Pharmacy, University of Arizona, Tucson, AZ, 1992.

[46] R.M. Dessau, J.L. Schlenker, J.B. Higgins, Framework topology of AlPO4-8: the first 14-ring molecular sieve, Zeolites 10 (1990) 522–524, https://doi.org/10.1016/S0144-2449(05)80306-9.

[47] R.F. Lobo, M. Tsapatsis, C.C. Freyhardt, S. Khodabandeh, P. Wagner, C.-Y. Chen, K. J. Balkus, S.I. Zones, M.E. Davis, Characterization of the extra-large-pore zeolite UTD-1, J. Am. Chem. Soc. 119 (1997) 8474–8484, https://doi.org/10.1021/ja9708528.

[48] K.G. Strohmaier, D.E.W. Vaughan, Structure of the first silicate molecular sieve with 18-ring pore openings, ECR-34, J. Am. Chem. Soc. 125 (2003) 16035–16039, https://doi.org/10.1021/ja0371653.

[49] M.Y. Jeon, D. Kim, P. Kumar, P.S. Lee, N. Rangnekar, P. Bai, M. Shete, B. Elyassi, H. S. Lee, K. Narasimharao, S.N. Basahel, S. Al-Thabaiti, W. Xu, H.J. Cho, E.O. Fetisov, R. Thyagarajan, R.F. DeJaco, W. Fan, K.A. Mkhoyan, J.I. Siepmann, M. Tsapatsis, Ultra-selective high-flux membranes from directly synthesized zeolite nanosheets, Nature 543 (2017) 690–694, https://doi.org/10.1038/nature21421.

[50] F. Cailliez, M. Trzpit, M. Soulard, I. Demachy, A. Boutin, J. Patarin, A.H. Fuchs, Thermodynamics of water intrusion in nanoporous hydrophobic solids, Phys. Chem. Chem. Phys. 10 (2008) 4817–4826, https://doi.org/10.1039/b807471b.

[51] A. Özgür Yazaydın, R.W. Thompson, Molecular simulation of water adsorption in silicalite: effect of silanol groups and different cations, Microporous Mesoporous Mater. 123 (2009) 169–176, https://doi.org/10.1016/j.micromeso.2009.03.045.

[52] L. Tzanis, M. Trzpit, M. Soulard, J. Patarin, High pressure water intrusion investigation of pure silica 1D channel AFI, MTW and TON-type zeolites, Microporous Mesoporous Mater. 146 (2011) 119–126, https://doi.org/10.1016/j.micromeso.2011.03.043.

[53] A.M. Norton, D. Kim, W. Zheng, N. Akter, Y. Xu, S.A. Tenney, D.G. Vlachos, M. Tsapatsis, J.A. Boscoboinik, Reversible formation of silanol groups in two-dimensional siliceous nanomaterials under mild hydrothermal conditions, J. Phys. Chem. C 124 (2020), https://doi.org/10.1021/acs.jpcc.0c03875, 18045–18053.

[54] R. Xiong, S.I. Sandler, D.G. Vlachos, Alcohol adsorption onto silicalite from aqueous solution, J. Phys. Chem. C 115 (2011) 18659–18669, https://doi.org/10.1021/jp205312k.